The influence of estrogen deficiency on the structural and mechanical properties of rat cortical bone

Anna Shipov[1], Paul Zaslansky[2], Heinrich Riesemeier[3], Gilad Segev[1], Ayelet Atkins[4], Noga Kalish-Achrai[1], Stephen Weiner[5] and Ron Shahar[1]

[1] Koret School of Veterinary Medicine, The Hebrew University of Jerusalem, Rehovot, Israel
[2] Department for Operative and Preventive Dentistry. Centrum für Zahn-, Mund- und Kieferheilkunde, Charité - Universitätsmedizin Berlin, Berlin, Germany
[3] BAM Federal Institute for Materials Research and Testing, Berlin, Germany
[4] Department of Chemistry and Bar Ilan Institute of Nanotechnology and Advanced Materials (BINA), Bar-Ilan University, Ramat Gan, Israel
[5] Department of Structural Biology, Weizmann Institute of Science, Rehovot, Israel

Corresponding author
Anna Shipov,
anna.shipov@mail.huji.ac.il

ABSTRACT

Background. Post-menopausal osteoporosis is a common health problem worldwide, most commonly caused by estrogen deficiency. Most of the information regarding the skeletal effects of this disease relates to trabecular bone, while cortical bone is less studied. The purpose of this study was to evaluate the influence of estrogen deficiency on the structure and mechanical properties of cortical bone.

Methods. Eight ovariectomized (OVH) and eight intact (control) Sprague Dawley rats were used. Structural features of femoral cortical bone were studied by light microscopy, scanning electron microscopy and synchrotron-based microcomputer-tomography and their mechanical properties determined by nano-indentation.

Results. Cortical bone of both study groups contains two distinct regions: organized circumferential lamellae and disordered bone with highly mineralized cartilaginous islands. Lacunar volume was lower in the OVH group both in the lamellar and disorganized regions ($182 \pm 75\,\mu m^3$ vs $232 \pm 106\,\mu m^3$, $P < 0.001$ and $195 \pm 86\,\mu m^3$ vs. $247 \pm 106\,\mu m^3$, $P < 0.001$, respectively). Lacunar density was also lower in both bone regions of the OVH group ($40 \pm 18 \times 10^3$ lacunae/mm^3 vs. $47 \pm 9 \times 10^3$ lacunae/mm^3 in the lamellar region, $P = 0.003$ and $63 \pm 18 \times 10^3$ lacunae/mm^3 vs. $75 \pm 13 \times 10^3$ lacunae/mm^3 in the disorganized region, $P < 0.001$). Vascular canal volume was lower in the disorganized region of the bone in the OVH group compared to the same region in the control group ($P < 0.001$). Indentation moduli were not different between the study groups in both bone regions.

Discussion. Changes to cortical bone associated with estrogen deficiency in rats require high-resolution methods for detection. Caution is required in the application of these results to humans due to major structural differences between human and rat bone.

INTRODUCTION

Osteoporosis is a common metabolic bone disorder affecting millions of people worldwide with significant health, quality of life and financial consequences (*Burge et al., 2007*). Osteoporosis is characterized by decreased bone strength and increased risk of fracture, and is often manifested by low bone mass (*Johnell & Kanis, 2005*). However, osteoporosis is a multifactorial disease, and low bone mass alone does not account for increased skeletal fragility (*Aspray et al., 1996*). The vague term "bone quality" is often used to describe the ensemble of properties that influence the ability of bone to resist fracture. It is now believed that poor bone quality associated with osteoporosis is due to a combination of deteriorated bone material properties and micro-architectural disruption, leading to a tendency for bone failure (*Aspray et al., 1996*). The factors responsible for the deterioration of the material properties of osteoporotic bone include changes in the mechanical properties and mineral density of the bone material (*Ma et al., 2008*) and alterations in the size and density of osteocytic lacunae, which were shown to be associated with accumulation of micro-cracks (*Vashishth et al., 2000*).

Estrogen has several effects on bone metabolism, including down regulation of bone remodeling and maintenance of the balance between bone deposition and resorption (*Riggs, Khosla & Melton 3rd, 2002*). Postmenopausal estrogen deficiency has marked effects on both trabecular and cortical bone and plays a crucial role in osteoporosis and osteoporotic fractures. Estrogen deficiency increases bone turnover and may impair bone formation, resulting in net bone loss, while estrogen replacement therapy results in an increase of both cancellous and cortical bone volume in women suffering from postmenopausal osteoporosis (*Khastgir et al., 2001*; *Wells et al., 2002*).

Rats are one of the most frequently used animal models for studying the various aspects of osteoporosis (*Jee & Yao, 2001*). However, it has been previously shown that the basic structure of the cortical bone of rat femora differs substantially from human cortical bone (*Bach-Gansmo et al., 2013*; *Shipov et al., 2013*). Specifically, while the cortices of long bones of humans are primarily osteonal, rat cortical bone contains very few osteons and consists primarily of two distinct elements, which exhibit different structural, mechanical and compositional properties. One element consists of ordered circumferential lamellae, which are located in the endosteal and/or periosteal regions of the bone, and are presumably the product of normal bone modeling processes. The other structural element is characterized by a disorganized architecture, and is centrally located within the cortex, surrounded externally and/or internally by the circumferential lamellar bone tissue. Another structure unique to cortical bone of rats and mice are 'islands' of calcified cartilage which are present only in the disordered region and are most likely remnants of early endochondral ossification processes (*Bach-Gansmo et al., 2013*; *Shipov et al., 2013*).

Since bone is a hierarchical material, alterations that occur at the macro-, micro- and nano-scale can dominate its overall mechanical and structural properties. Such changes determine the so-called "bone quality" in healthy and diseased bone tissue. It is therefore important to obtain an insight into the structural and mechanical changes that occur at different hierarchical levels of cortical bone, when studying the effects of estrogen

deficiency. Specifically, in rat cortical bone it is necessary to study the two distinct structural components (the disorganized region and the lamellar regions) separately, since these two tissues have markedly different structural and mechanical properties, and it is reasonable to assume that estrogen deficiency may affect them differently.

Cortical bone is known to be the major determinant of bone strength (*Holzer et al., 2009*; *Ito et al., 2002*). Nevertheless the majority of studies of osteoporosis are conducted on cancellous (trabecular) bone, while there are fewer studies investigating cortical bone. Furthermore, previous studies examining the effects of ovariectomy on cortical bone in rats reported conflicting results (*De Carvalho et al., 2012*; *Miyagawa et al., 2011*; *Peng et al., 1997*).

The aim of this study was to investigate the influence of estrogen deficiency on the structure and mechanical properties of rat cortical bone at the micro- and nano- scales in the two bone types: lamellar and disorganized cortical bone. This aim was achieved by comparing the structural and material properties of femoral cortical bone between ovariectomized and non-ovariectomized rats using nanoindentation, light microscopy, scanning electron microscopy, and synchrotron based micro-tomography.

MATERIALS AND METHODS

Animals

Sixteen female Sprague Dawley rats were used in this study. They were divided into two groups: eight rats were ovariectomized at eight weeks of age (OVH group), and eight rats were left intact (control group). All rats were allowed access to standard rodent chow and water ad libitum, subjected to a 12-h light:dark cycle, and raised in individual cages in the same room. At the age of 8 months, all 16 rats were sacrificed by CO_2 exposure.

The rats used here were part of another, much larger long-term study that investigated the effect of ovariectomy on cortical and cancellous bone using sequential injections of fluorochromes. Ethical approval to that study was given by the national committee for animal experimentation, approval # IL-12-03-047.

Samples

Both femora were harvested for cortical bone analysis within two hours of sacrifice. Soft tissue was carefully removed from the bones, which were wrapped in saline-soaked gauze and stored at −20 °C until further testing.

Light microscopy

Right femora of three OVH and three control rats were used for light microscopy studies. Six ∼1 mm thick cross-sectional (transverse) samples equally distributed along the length of the bone were prepared from the diaphysis of each femur (Fig. 1A) using a diamond-blade water-cooled saw (Isomet® low speed saw; Buhler, Minneapolis, MN, Minneapolis, MN, USA). Each slice was marked such that its axial position as well as its proximal, medial and cranial aspects were clearly identified. The slices were ground using a grinding-polishing device (Minimet®1000; Buehler, Minneapolis, MN, USA) using a series of abrasive papers (increasing from 200 to 4000 grit), followed by polishing with cloths and 3 μm
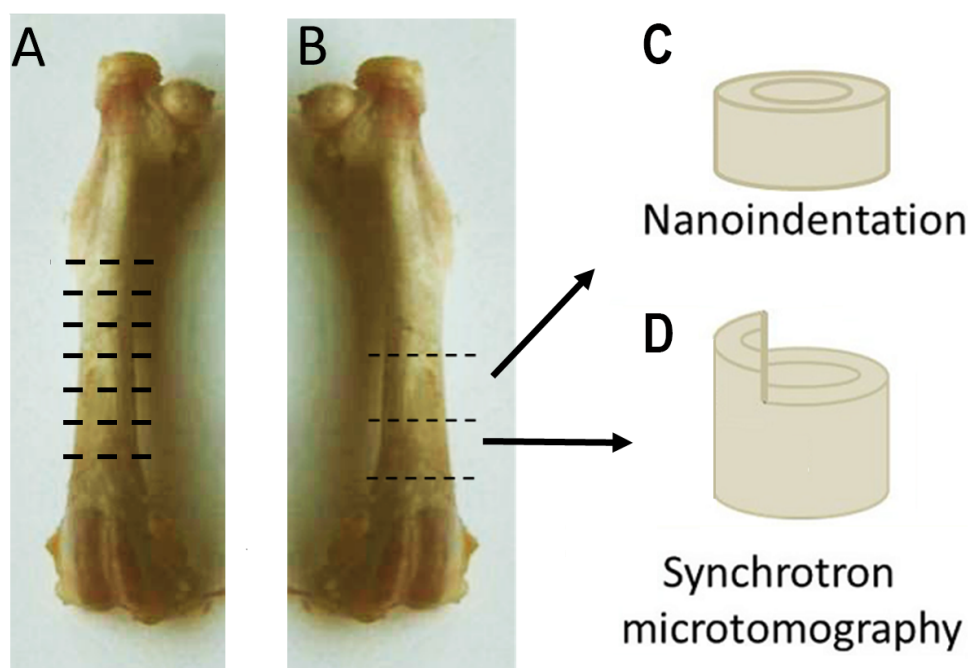
Figure 1 Sample preparation. (A) Structural features of the cortex were studied with light microscopy. Six ~1 mm-thick cross-sectional samples were prepared from the diaphysis of the right femur, equally distributed along the length of the bone. (B) Two 2 mm-thick cross-sections of the distal shaft were prepared from the left femora. The proximal section was used for nanoindentation (C), While the distal for synchrotron based microtomography (D). Part of the proximal half of the circumference of each sample used for microtomography was removed, leaving a 1 × 1 × 1 mm protuberance above the circumference of the cortex.

and 1 μm diamond paste. The polished bone surfaces were imaged using reflected-light microscopy (Olympus® BX-51 microscope, Olympus, Japan). Images were captured using a 12.1 megapixel-resolution camera attached to the microscope (Olympus® DP 71 digital camera, Olympus, Japan) and analyzed using image analysis software (ImageJ, NIH 1.47, USA).

Synchrotron Micro-CT

Small (two mm long) cylindrical samples were prepared from the distal shaft of eight left femora of each group for multi-resolution imaging by monochromatic synchrotron radiation radiography available at the BAMline beamline of the BESSY II storage ring of the Helmholtz-Zentrum Berlin für Materialien und Energie (HZB). Part of the proximal half of the circumference of each sample was removed (using a dental burr), leaving a 1 × 1× 1 mm protuberance above the circumference of the cortex (see Fig. 1B). The samples were scanned at two resolutions: the lower half of each sample, which contained the entire circumferences of the cortex, was scanned at a resolution of 4.35 μm effective pixel size, and the upper half of each sample, consisting of the protuberance, was scanned at an effective pixel size of 1.75 μm. The samples were mounted upright on the rotation stage of BAMline (*Rack et al., 2008*), and scanned in absorption mode using the double

multilayer monochromator (DMM) centered at an energy of 23 keV. Tomographic datasets were obtained by rotating the samples by 180° at angular increments of 0.24°, obtaining 720∼750 projection (shadow) images per scan.

For void volume analysis an enhanced contrast imaging mode was used by in-line phase contrast for which 750 projection images were recorded at angular increments of 0.24° using an energy of 18 keV with a sample-to-detector distance of 25 mm. The radiograms were background-corrected by normalization with empty beam (flat-field) images, obtained intermittently, after subtraction of dark-current images. Reconstruction into 3-D datasets was performed using the PyHST reconstruction package from the ESRF (Grenoble, France).[11]

Structural 3-D data were analyzed using ImageJ (ImageJ, NIH, 1.47, USA) (*Bolte & Cordelieres, 2006*). In each bone sample 5–14 neighboring volumes of interest (VOI), ranging in size between 0.0022–0.039 mm^3, were selected, such that each VOI consisted exclusively of either lamellar bone or disorganized bone. Since the signal-to-noise ratio and acquisition parameters were optimized for density and size of our samples, excellent contrast between bone and void was obtained, and automatic thresholding using the Otsu algorithm was sufficient to binarize the images of each VOI, separating it into 'bone' (white) and 'void' (black) entities (*Nuzzo et al., 2002*; *Shipov et al., 2013*). Next, the volumes of all voids within the VOI were measured using the ImageJ plugin "Object Counter 3D" (*Bolte & Cordelieres, 2006*). Based on values of osteocyte lacunar volumes reported in the literature (*Hannah et al., 2010*; *McCreadie et al., 2004*; *Shipov et al., 2013*; *Tommasini et al., 2012*) and on the distribution of the sizes of voids in our study, voids within the bone matrix with volumes ranging between 75–625 μm^3 were considered to be osteocytic lacunae, while voids larger than 625 μm^3 were considered to represent vascular canals. The data were used to determine mean lacunar volume and lacunar density. Bone porosity was calculated for each VOI from the ratio of total void volume to VOI volume. Small voids, such as canaliculi, were not included in the analysis since their size is below the detection limit at the resolutions used in this study.

In order to allow valid comparisons between mean values of vascular canal volume (mm^3) and vascular canal density (number of canals per mm^3) determined in different-sized VOIs, normalization is required [see a detailed description in a paper by Shipov and colleagues (*Shipov et al., 2013*). Briefly, normalization can be achieved by two alternative approaches: The first approach assumes that when a VOI increases in volume the vascular canals in the original VOI simply extend into the larger VOI, therefore their volume increases, but their number does not change. The second approach assumes that the mean vascular canal volume in the larger VOI is the same as in the original VOI, but the number of canals increases. We chose a hybrid approach, in which we assume that both the number and volume of the vascular canals increases when the VOI increases, by the square root of the ratio between the VOI volumes, thus maintaining the volume fraction of the canals. We note that since the size of individual lacunae is relatively uniform and not affected by the differences in the size of the VOI, this normalization was not required when calculating mean lacunar volume and lacunar density.

Mineral density in different regions of the scanned bone was determined by calibrating attenuation values based on scans of 2 standardized phantoms (Bruker-CT, Kontich, Belgium) with known mineral density (0.25 g/cm^{-3} and 0.75 g/ cm^{-3}). The density-attenuation relationship was assumed to be linear and the mean attenuation values of the two phantoms was used to create a tissue mineral density (TMD)-attenuation calibration curve. For each particular VOI, its TMD was calculated by determining the mean X-ray attenuation and using the calibration curve.

Volumes of interest were selected within the lamellar region, disorganized region and calcified cartilage islands.

Some of the specimens in the control group were previously analyzed in a different project (*Shipov et al., 2013*). These specimens were re-analyzed, using new VOIs to correspond to the VOIs in the OVH group.

Mechanical testing: Nanoindentation

Three transverse sections from the left femoral mid-shaft of three rats in each group were used for nanoindentation experiments (Fig. 1B). The sections were dehydrated with increasing concentrations of ethanol, then embedded for eight hours in methylmethacrylate (MMA) which was polymerized in an oven at 60 °C. The embedded samples were cut with a diamond saw (Leica SP1600 saw-microtome) to a thickness of one mm, then ground and polished to create plano-parallel surfaces free of scratches and polishing damage.

Nanoindentation was performed using a scanning nanoindenter (TI950 Triboindenter, Hysitron Inc., Minneapolis, MN, USA) with a Berkovich diamond indenter tip. The nanoindenter was programmed to perform a scan of the surface, consisting of 2 lines 20 μm apart, with each line having an indent spacing of 10 μm, leading to a total of 120 indents in each sample. The following load function was used: maximum load of 5,000 μN, loading rate at 1,000 μN/s, holding at maximum force for 60 s and unloading to 1,000 μN at a rate of 400 μN/s, followed by a second holding time of 10 s and finally unloading to 0 μN at a rate of 200 μN/s. Measured properties included peak load, peak displacement and stiffness. The indentation modulus was calculated using the Oliver-Pharr method (*Oliver & Pharr, 1992*), based on the slope of the unloading curve in the region between 20% and 95% of the maximum load (*Lewis & Nyman, 2008*). The specimens in the control group were previously analyzed for a different project (*Shipov et al., 2013*) and used as a control in the current project.

Scanning electron microscopy

Following nanoindentation, the same samples were imaged (uncoated) in an environmental scanning electron microscope (ESEM, FEG Quanta 600, FEI, Eindhoven, The Netherlands) with a backscattered electron detector, using an acceleration voltage of 15 kV in low vacuum mode. Indentations within the bone were identified and categorized in terms of the structural element in which they were carried out (i.e., lamellar, disorganized or cartilaginous islands, Figs. 2B, 2C). Indents that were performed in PMMA or in the proximity of drying cracks or other voids were excluded from the analysis.
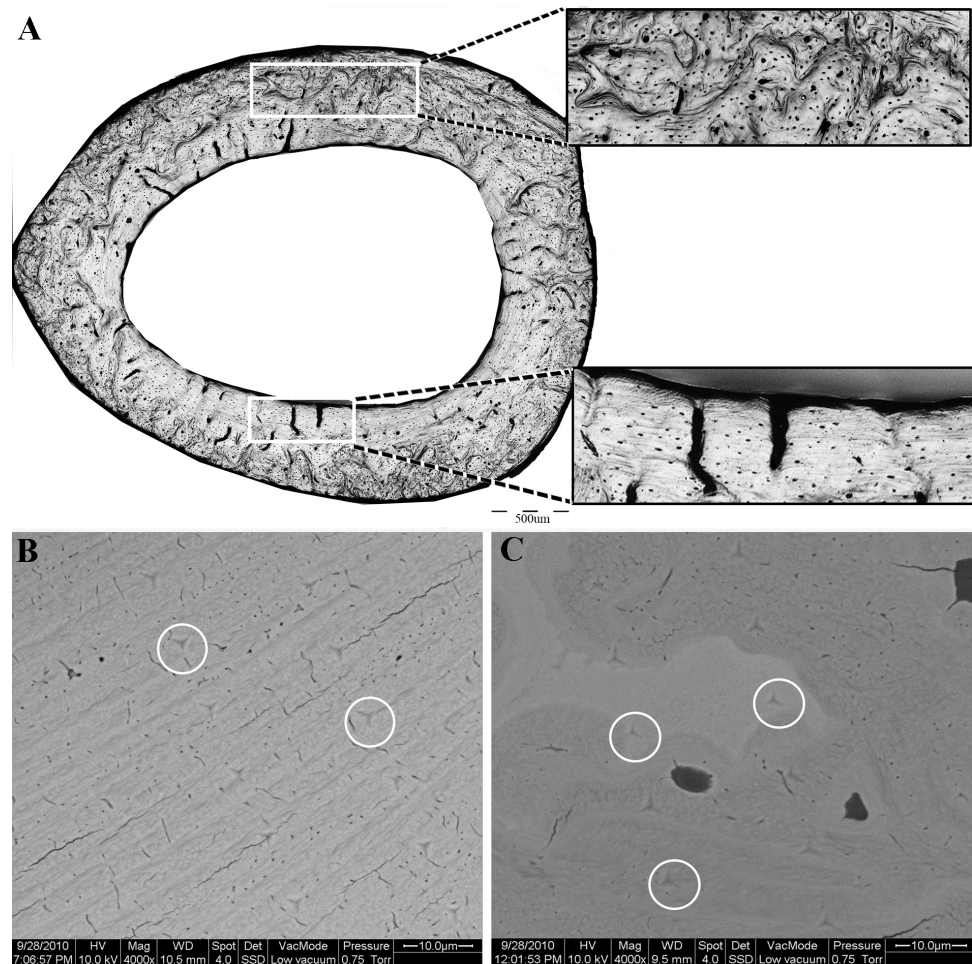
Figure 2 (A) **Light microscopy, showing the two distinct regions of the proximal femoral cortex characteristic of both the OVH and control groups.** Upper insert- disorganized bone. Lower insert—lamellar bone. (B, C) Scanning electron microscopy of the lamellar (B) and disorganized (C) regions of the bone. White circles delineate the indents of the nanoindentation experiment.

Statistical analysis

Normality of distribution was assessed using the Shapiro–Wilk test. Normally distributed data are presented as mean ± SD. Continuous variables were compared between two groups using the Student's t-test or the Mann–Whitney U-test based on data distribution. Continuous variables (e.g., lacunar volume, lacunar density etc.) that were measured multiple times in each bone were compared between the groups using the generalized estimating equations (since we had multiple measurements from the same bone, and therefore each one of these measurements could not be considered an independent measurement). For all tests, $P < 0.05$ was considered statistically significant. All calculations were performed using a commercially available statistical software package (SPSS 17.0 for Windows, Chicago, IL, USA).

Table 1 Results of synchrotron-based microtomography (Data presented as mean ± SD). Comparisons were made separately for the different bone regions between OVH and control groups.

Parameter	OVH		Control	
	Lamellar	Disorganized	Lamellar	Disorganized
Vascular canal volume (μm^3)	$159 \pm 374 \times 10^3$	$62 \pm 168 \times 10^{3**}$	$156 \pm 374 \times 10^3$	$93 \pm 314 \times 10^3$
Lacunar volume (μm^3)	$182 \pm 75^{**}$	$195 \pm 86^{**}$	232 ± 106	247 ± 106
Vascular canal density (canals/mm^3)	$129 \pm 56^{**}$	$241 \pm 95^*$	134 ± 84	209 ± 91
Lacunar density (lacunae/mm^3)	$40 \pm 18 \times 10^{3*}$	$63 \pm 18 \times 10^{3**}$	$47 \pm 9 \times 10^3$	$75 \pm 13 \times 10^3$
Porosity %	$2.79 \pm 1.57^*$	$2.74 \pm 0.77^{**}$	3.23 ± 1.06	3.83 ± 1.31

Notes.

[*]Significant (< 0.05) differences between OVH and control.

[**]Significant (≤ 0.001) differences between OVH and control.

RESULTS

Morphology and structural properties

Light microscopy

All cortical cross sections, in both the OVH and control groups, clearly revealed two distinct microstructural regions (Fig. 2). One region consisted of circumferential lamellae and was located in the endosteal and/or periosteal aspect of the cross section. The other region had a non-lamellar, disorganized appearance and occupied the central part of the cortical cross-section. Highly mineralized islands of irregular shape, previously shown to consist of mineralized cartilage, appeared in the disorganized region (*Bach-Gansmo et al., 2013*; *Shipov et al., 2013*).

Synchrotron based microtomography

Synchrotron based microtomography scans were analyzed to compare mean lacunar volume, mean vascular canal volume and vascular canal density between the study groups for each bone type (disorganized and lamellar, Table 1, Fig. 3). Lacunar volume and density was significantly lower in the OVH group compared to the control group, in both the lamellar and disorganized regions ($P < 0.001$). Vascular canal volume was lower in the disorganized region in the OVH group compared to the same region in the control group, while no difference was found between the groups in vascular canal density, in both the lamellar and disorganized regions of the bone (Table 1).

Mechanical properties

Mechanical properties at different locations of the bone material were measured by nano-indentation. Indentation moduli of the cartilaginous islands in the control group were higher compared to those in the OVH group (33.40 ± 2.8 GPa vs. 29.8 ± 3.2 GPa, $P = 0.03$). There was no difference in the modulus of the lamellar region between the study groups (28.5 ± 3.0 GPa vs. 27.8 ± 4.3 GPa, $P = 0.7$), nor was there a difference in the modulus of the disorganized region between the study groups (30.1 ± 3.5 GPa vs. 28.1 ± 3.9 GPa, $P = 0.17$). Within each group (OVH and control), the cartilaginous islands had the highest modulus, followed by the disorganized region of the bone, while the lamellar region had the lowest indentation modulus.
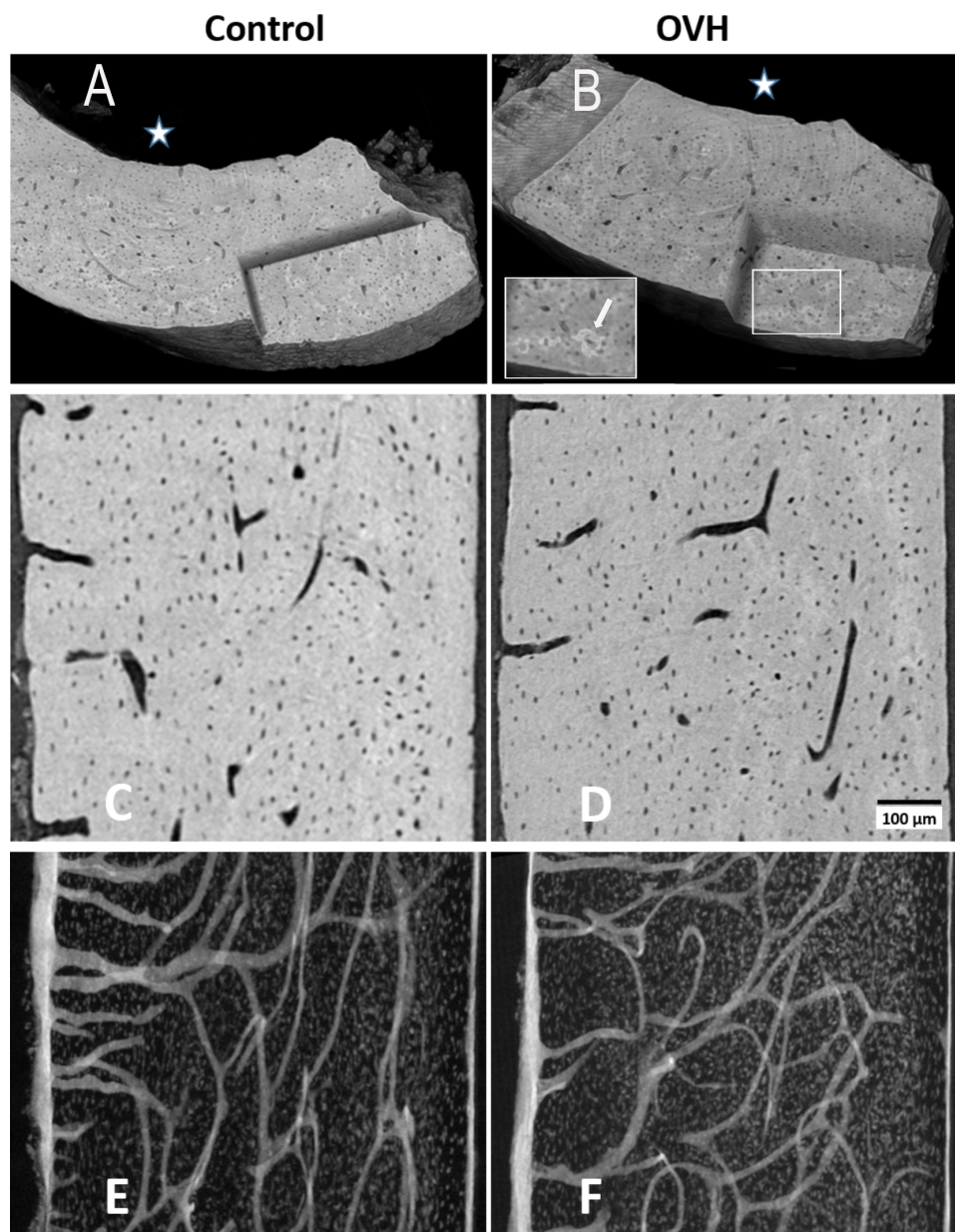
Figure 3 **Typical views of synchrotron microCT data of control and of ovarictomized rats.** (A and B) show 3D renderings of part of typical cortices of both groups, in which a corner is virtually cut out, to reveal parts of the internal bone structures. White star identifies the endosteal side of the bones. Cartilaginous islands within the bone can be identified by the higher mineral content (brighter color, insert B, white arrow). (C and D) show typical 3 μm thick tomography slices, where both osteocyte lacunae and vascular canals are clearly visible. (E and F) highlight the distribution of voids in axial slices along the bone shaft within a 125 μm thick slice. Vascular canal silhouettes appear to enter the bone at right angles to the endosteal bone surface (left hand side), and run both longitudinally and radially in the central bone region.

Mineral density

Tissue mineral density (TMD) was found to be similar in both groups in both the lamellar and disorganized regions. However, within each study group, significant differences were detected between the TMD of the two bone types (lamellar and disorganized), with the cartilaginous islands having the highest TMD (1.52 ± 0.05 g/cm^3 in the OVH and 1.53 ± 0.04 g/cm^3 in the control group, $P = 0.363$), followed by the disorganized region (1.40 ± 0.03 g/cm^3 in the OVH and 1.41 ± 0.03 g/cm^3 in the control group, $P = 0.695$) while the lamellar region had the lowest mineral density (1.37 ± 0.05 g/cm^3 in the OVH and 1.36 ± 0.06 g/cm^3, $P = 0.134$).

DISCUSSION

Here we show that ovariectomy in rats affects the structure and mechanical properties of the cortical bone. However, the changes we found were minor and their detection required high-resolution methods. The changes included an overall decrease in osteocyte lacunar volume and density, as well as lower vascular canal volume in the disorganized region of the bone material. These changes may affect the ability of cortical bone to respond to mechanical stimuli and maintain its health.

Osteocytes reside in lacunae embedded within the matrix of mature bone. It is widely believed that osteocytes play a crucial role in maintaining the health and mechanical function of bone by regulating the modeling and remodeling processes (*Lanyon, 1993*). Though extensive data regarding lacunar size are lacking, it has been shown that lacunae in mice become smaller with age (*Heveran et al., 2018*) and that smaller lacunae are associated with decreased response to mechanical loading (*Hemmatian et al., 2018*), indicating the importance of lacunar size in bone health. Previous studies comparing lacunar size in cortical bone of OVH vs. non-OVH rats had conflicting results. A study utilizing confocal microscopy did not find a difference in lacunar volumes in the proximal tibia six weeks after ovariectomy (*Sharma et al., 2012*), while others, using SRμCT, reported smaller lacunar volume in the endosteal region of the femoral cortical bone seven months after ovariectomy (*Tommasini et al., 2012*). We found that lacunae in OVH rats were significantly smaller in both the lamellar and disorganized regions. These morphological changes following OVH could affect the function of the osteocytic-canicular system by impairing cell-to-cell communication and thus reducing the effectiveness of the osteocyte in mechano-sensing and damage repair, affecting the health of cortical bone in the long term.

Lacunar density is another parameter with major functional significance (*Qiu et al., 2003*; *Vashishth et al., 2000*). It has been shown that adequate numbers of osteocytes are essential for micro-damage sensing and removal (*Busse et al., 2010*). Furthermore, their density within the bone material positively correlates with anabolic activity of osteoblasts and the biomechanical quality of the bone, and negatively correlates with osteoclast activity and micro-damage sensing and accumulation (*Ma et al., 2008*; *Qiu et al., 2005*). In addition, osteocytic lacunae have been shown to affect crack propagation properties in bone and a lower density of osteocytes was found in patients with fractures compared to healthy controls (*Qiu et al., 2003*). Finally, estrogen deficiency is associated with osteocyte

apoptosis in humans and rodents (*Almeida et al., 2007*; *Tomkinson et al., 1997*) while in sheep, it has been shown that in addition to decrease in lacunar density, the number of empty lacunae (lacunae that do not contain viable osteocytes) is almost twice as high in osteoporotic bone (*Zarrinkalam et al., 2012*). Our study demonstrates a ∼15% decrease in lacunar density in both the ordered and disordered regions of the cortical bone in OVH group. Since our analysis is based on synchrotron micro-tomography, we can only identify lacunae and determine their size and density, and cannot determine osteocyte viability. It is therefore possible that in the OVH group, there are not only fewer and smaller lacunae than in the control group, but also that some of these lacunae do not contain viable osteocytes due to increased apoptosis (*Zarrinkalam et al., 2012*). These effects may reduce the efficiency of the osteocytic network even further. Though lacunar mineralization in rats has so far not been reported, it is nevertheless possible that following apoptosis of osteocytes some of the lacunae become mineralized and merge with the surrounding matrix, as has been reported in aging human bone and in the zebrafish skeleton (*Busse et al., 2010*; *Ofer et al., 2019*).

All the above-mentioned alterations in osteocyte size, density and possibly viability, can potentially affect the ability of cortical bone to sense damage, maintain its health and allow accelerated damage accumulation, thus increasing bone fragility. It is plausible that in humans these changes occur over time and eventually become crucial as damage accumulates. However, such damage is less likely to become significant and detectable during a short-term experiment, or even during the entire life span of rats, which is much shorter than the life span of humans. This may account for the minimal differences in the mechanical properties observed between the OVH and control groups, and further emphasizes the shortcomings of rodents as a model for bone pathologies in humans.

Bone porosity is another characteristic of bone, which is a major determinant of its quality. The porosity of the disorganized region was higher in the control group, probably due to the larger volume of vascular canals found in this group. We note however, that cortical porosity was relatively low in all areas of both groups (between 2.8% and 3.8%). Sharma and colleagues (*Sharma et al., 2018*) reported that estrogen deficiency causes an increase in cortical bone vascular porosity in the proximal tibial metaphysis of rats, with enlarged vascular pores, but little change in tissue mineral density. However, studies reporting the effect of estrogen deficiency on the cortical bone of the rat (*Sharma et al., 2012*; *Stern et al., 2018*) have not investigated the effects separately in the two distinct zones of the bone (lamellar vs. disorganized) and the duration of these studies was short (weeks after ovariectomy), while the results reported here were found 6 months after OVH was performed.

Previous studies investigating the effects of ovariectomy on the stiffness of the bone material of rat cortical bone have reported inconsistent results. Some studies found decreased stiffness (*Peng et al., 1997*), while others found no change (*Miyagawa et al., 2011*) or even increased bone material stiffness following ovariectomy (*De Carvalho et al., 2012*). Other studies found a site specific or time-dependent effect, with initially superior mechanical properties of cortical bone in control rats, which disappears with time (12–28 weeks post OVH) (*Peng et al., 1997*). We found no difference in stiffness

between the control and OVH groups in the lamellar and disorganized regions, and only mild differences in the material stiffness of the cartilaginous islands of the bone. We note however that this difference, although small, could affect mechanical properties such as fatigue resistance, which were not studied here.

One of the characteristics of post-menopausal osteoporosis in women is a disruption of the fine balance between bone deposition and resorption. It has been shown that in post-menopausal women bone resorption can increase by 90% while bone formation increases only by 45%, producing a net negative effect, thus decreasing its stiffness and mineral density (*Garnero et al., 1996*). Since the bones of small rodents such as mice and rats do not undergo significant cortical bone remodeling (*Baron, Tross & Vignery, 1984*; *Erben, 1996*), this may explain the lack of significant differences seen in mechanical properties and mineral density between the OVH and control study groups.

This study has several limitations. First, the number of animals used was relatively small, and larger groups could lead to strengthening of some of the statistical comparisons. Second, due to differences in bone structure between rats and human patients, the relevance of the results of this study with regard to humans is questionable and additional studies, evaluating these changes in a model animal that more closely simulates the human skeleton, are warranted.

In conclusion, we found that the effect of low estrogen levels on the cortical bone of rats is manifested by a lower density of osteocytic lacunae, which are also smaller, both in the lamellar and disorganized regions of the bone. These changes could lead to slow deterioration in bone quality, which might not be clinically manifested due to the short life span of rats. We note that the basic structure of rat cortical bone is markedly different from that of human cortical bone, since it does not undergo remodeling (while imbalance in the remodeling activity is considered the main cause of human osteoporosis), thus raising concerns as to the frequent use of rat cortical long bone as a model for human bone diseases.

ACKNOWLEDGEMENTS

We wish to express our gratitude to the Max Planck Institute of colloids and interfaces, department of biomaterials, Potsdam, Germany for allowing us to use their facilities. We would also like to thank Petra Leibner, Birgit Schonert and Anne-marie Martens for their assistance in the technical aspects of this project. The authors would like to express special thanks to Professor Peter Fratzl and the late Professor John Currey for most helpful discussions. We thank the Helmholtz-Zentrum Berlin für Materialien und Energie for allocation of synchrotron radiation beamtime.

Funding

This work was supported by the German research foundation (DFG) through SPP1420 and the Helmholtz-Zentrum Berlin by allocation of synchrotron radiation beamtime. The

funders had no role in study design, data collection and analysis, decision to publish, or preparation of the manuscript.

Grant Disclosures

The following grant information was disclosed by the authors:

German research foundation (DFG): SPP1420.

The Helmholtz-Zentrum Berlin by allocation of synchrotron radiation beamtime (proposal 2011_1_101141).

Competing Interests

The authors declare there are no competing interests.

Author Contributions

- Anna Shipov, Paul Zaslansky, Gilad Segev and Ron Shahar conceived and designed the experiments, performed the experiments, analyzed the data, prepared figures and/or tables, authored or reviewed drafts of the paper, and approved the final draft.
- Heinrich Riesemeier conceived and designed the experiments, performed the experiments, analyzed the data, authored or reviewed drafts of the paper, and approved the final draft.
- Ayelet Atkins and Noga Kalish-Achrai performed the experiments, analyzed the data, authored or reviewed drafts of the paper, and approved the final draft.
- Stephen Weiner conceived and designed the experiments, authored or reviewed drafts of the paper, and approved the final draft.

Data Availability

Data retrieved from the micro-CT scans and indentation are available in the Supplemental Files.

Additional data is available at Morphosource and Figshare: http://www.morphosource.org/Detail/ProjectDetail/Show/project_id/1182.

Shipov, Anna (2020): peerj-30209-blood_vessel_volume (1).xlsx. figshare. Dataset. https://doi.org/10.6084/m9.figshare.13204370.v1.

Shipov, Anna (2020): peerj-30209-lacunae_and_blood_vessel_volume_and_number_of_lacunae_and_vessels_per_volume_and_porosity (1).xlsx. figshare. Dataset. https://doi.org/10.6084/m9.figshare.13204373.v1.

Shipov, Anna (2020): peerj-30209-nanoindentation.xlsx. figshare. Dataset. https://doi.org/10.6084/m9.figshare.13204376.v1.

Shipov, Anna (2020): peerj-30209-lacunae_nOVH_and_OVH_for_stats (1).xlsx. figshare. Dataset. https://doi.org/10.6084/m9.figshare.13204379.v1.

Supplemental Information

Supplemental information for this article can be found online at http://dx.doi.org/10.7717/peerj.10213#supplemental-information.

REFERENCES

Almeida M, Han L, Martin-Millan M, Plotkin LI, Stewart SA, Roberson PK, Kousteni S, O'Brien CA, Bellido T, Parfitt AM, Weinstein RS, Jilka RL, Manolagas SC. 2007. Skeletal involution by age-associated oxidative stress and its acceleration by loss of sex steroids. *Journal of Biological Chemistry* **282**:27285–27297 DOI 10.1074/jbc.M702810200.

Aspray TJ, Prentice A, Cole TJ, Sawo Y, Reeve J, Francis RM. 1996. Low bone mineral content is common but osteoporotic fractures are rare in elderly rural Gambian women. *Journal of Bone and Mineral Research* **11**:1019–1025.

Bach-Gansmo FL, Irvine SC, Bruel A, Thomsen JS, Birkedal H. 2013. Calcified cartilage islands in rat cortical bone. *Calcified Tissue International* **92**:330–338 DOI 10.1007/s00223-012-9682-6.

Baron R, Tross R, Vignery A. 1984. Evidence of Sequential Remodeling in Rat Trabecular Bone - Morphology, Dynamic Histomorphometry, and Changes during Skeletal Maturation. *Anatomical Record* **208**:137–145 DOI 10.1002/ar.1092080114.

Bolte S, Cordelieres FP. 2006. A guided tour into subcellular colocalization analysis in light microscopy. *Journal of Microscopy-Oxford* **224**:213–232 DOI 10.1111/j.1365-2818.2006.01706.x.

Burge R, Dawson-Hughes B, Solomon DH, Wong JB, King A, Tosteson A. 2007. Incidence and economic burden of osteoporosis-related fractures in the United States, 2005–2025. *Journal of Bone and Mineral Research* **22**:465–475 DOI 10.1359/jbmr.061113.

Busse B, Djonic D, Milovanovic P, Hahn M, Puschel K, Ritchie RO, Djuric M, Amling M. 2010. Decrease in the osteocyte lacunar density accompanied by hypermineralized lacunar occlusion reveals failure and delay of remodeling in aged human bone. *Aging Cell* **9**:1065–1075 DOI 10.1111/j.1474-9726.2010.00633.x.

De Carvalho ACB, Fernandes GVO, Lima I, De Oliveira DF, Henriques HN, Pantaleao JAS, Granjeiro JM, Lopes RT, Guzman-Silva MA. 2012. Influence of estrogen deficiency and tibolone therapy on trabecular and cortical bone evaluated by computed radiography system in rats. *Acta Cirurgica Brasileira* **27**:217–222 DOI 10.1590/S0102-86502012000300003.

Erben RG. 1996. Trabecular and endocortical bone surfaces in the rat: modeling or remodeling? *Anatomical Record* **246**:39–46 DOI 10.1002/(SICI)1097-0185(199609)246:1<39::AID-AR5>3.0.CO;2-A.

Garnero P, SornayRendu E, Chapuy MC, Delmas PD. 1996. Increased bone turnover in late postmenopausal women is a major determinant of osteoporosis. *Journal of Bone and Mineral Research* **11**:337–349.

Hannah KM, Thomas CDL, Clement JG, De Carlo F, Peele AG. 2010. Bimodal distribution of osteocyte lacunar size in the human femoral cortex as revealed by micro-CT. *Bone* **47**:866–871 DOI 10.1016/j.bone.2010.07.025.

Hemmatian H, Jalali R, Semeins CM, Hogervorst JMA, vanLenthe GH, Klein-Nulend J, Bakker AD. 2018. Mechanical loading differentially affects osteocytes in fibulae from

lactating mice compared to osteocytes in virgin mice: possible role for lacuna size. *Calcified Tissue International* **103**:675–685 DOI 10.1007/s00223-018-0463-8.

Heveran CM, Rauff A, King KB, Carpenter RD, Ferguson VL. 2018. A new open-source tool for measuring 3D osteocyte lacunar geometries from confocal laser scanning microscopy reveals age-related changes to lacunar size and shape in cortical mouse bone. *Bone* **110**:115–127 DOI 10.1016/j.bone.2018.01.018.

Holzer G, Von Skrbensky G, Holzer LA, Pichl W. 2009. Hip fractures and the contribution of cortical versus trabecular bone to femoral neck strength. *Journal of Bone and Mineral Research* **24**:468–474 DOI 10.1359/jbmr.081108.

Ito M, Nishida A, Koga A, Ikeda S, Shiraishi A, Uetani M, Hayashi K, Nakamura T. 2002. Contribution of trabecular and cortical components to the mechanical properties of bone and their regulating parameters. *Bone* **31**:351–358 DOI 10.1016/S8756-3282(02)00830-X.

Jee WS, Yao W. 2001. Overview: animal models of osteopenia and osteoporosis. *Journal of Musculoskeletal Neuronal Interactions* **1**:193–207.

Johnell O, Kanis J. 2005. Epidemiology of osteoporotic fractures. *Osteoporosis International* **16**(**Suppl 2**):S3–S7 DOI 10.1007/s00198-004-1702-6.

Khastgir G, Studd J, Holland N, Alaghband-Zadeh J, Fox S, Chow J. 2001. Anabolic effect of estrogen replacement on bone in postmenopausal women with osteoporosis: histomorphometric evidence in a longitudinal study. *Journal of Clinical Endocrinology & Metabolism* **86**:289–295.

Lanyon LE. 1993. Osteocytes, strain detection, bone modeling and remodeling. *Calcified Tissue International* **53**(**Suppl 1**):S102–S106 DOI 10.1007/BF01673415.

Lewis G, Nyman JS. 2008. The use of nanoindentation for characterizing the properties of mineralized hard tissues: state-of-the art review. *Journal of Biomedical Materials Research Part B-Applied Biomaterials* **87B**:286–301 DOI 10.1002/Jbm.B.31092.

Ma YL, Dai RC, Sheng ZF, Jin Y, Zhang YH, Fang LN, Fan HJ, Liao EY. 2008. Quantitative associations between osteocyte density and biomechanics, microcrack and microstructure in OVX rats vertebral trabeculae. *Journal of Biomechanics* **41**:1324–1332 DOI 10.1016/j.jbiomech.2008.01.017.

McCreadie BR, Hollister SJ, Schaffler MB, Goldstein SA. 2004. Osteocyte lacuna size and shape in women with and without osteoporotic fracture. *Journal of Biomechanics* **37**:563–572 DOI 10.1016/S0021-9290(03)00287-2.

Miyagawa K, Kozai Y, Ito Y, Furuhama T, Naruse K, Nonaka K, Nagai Y, Yamato H, Kashima I, Ohya K, Aoki K, Mikuni-Takagaki Y. 2011. A novel underuse model shows that inactivity but not ovariectomy determines the deteriorated material properties and geometry of cortical bone in the tibia of adult rats. *Journal of Bone and Mineral Metabolism* **29**:422–436 DOI 10.1007/s00774-010-0241-9.

Nuzzo S, Peyrin F, Cloetens P, Baruchel J, Boivin G. 2002. Quantification of the degree of mineralization of bone in three dimensions using synchrotron radiation microtomography. *Medical Physics* **29**:2672–2681 DOI 10.1118/1.1513161.

Ofer L, Dumont M, Rack A, Zaslansky P, Shahar R. 2019. New insights into the process of osteogenesis of anosteocytic bone. *Bone* **125**:61–73 DOI 10.1016/j.bone.2019.05.013.

Oliver WC, Pharr GM. 1992. An improved technique for determining hardness and elastic-modulus using load and displacement sensing indentation experiments. *Journal of Materials Research* **7**:1564–1583 DOI 10.1557/Jmr.1992.1564.

Peng ZQ, Vaananen HK, Zhang HX, Tuukkanen J. 1997. Long-term effects of ovariec-tomy on the mechanical properties and chemical composition of rat bone. *Bone* **20**:207–212 DOI 10.1016/S8756-3282(96)00369-9.

Qiu SJ, Rao DS, Fyhrie DP, Palnitkar S, Parfitt AM. 2005. The morphological asso-ciation between microcracks and osteocyte lacunae in human cortical bone. *Bone* **37**:10–15 DOI 10.1016/j.bone.2005.01.023.

Qiu S, Rao DS, Palnitkar S, Parfitt AM. 2003. Reduced iliac cancellous osteocyte density in patients with osteoporotic vertebral fracture. *Journal of Bone and Mineral Research* **18**:1657–1663 DOI 10.1359/jbmr.2003.18.9.1657.

Rack A, Zabler S, Muller B, Riesemeier H, Weidemann G, Lange A, Goebbels J, Hentschel M, Gorner W. 2008. High resolution synchrotron-based radiography and tomography using hard X-rays at the MAMline (BESSY II). *Nuclear Instruments and Methods in Physics Research Section A* **586**:327–344 DOI 10.1016/j.nima.2007.11.020.

Riggs BL, Khosla S, Melton 3rd LJ. 2002. Sex steroids and the construction and conserva-tion of the adult skeleton. *Endocrine Reviews* **23**:279–302 DOI 10.1210/edrv.23.3.0465.

Sharma D, Ciani C, Marin PA, Levy JD, Doty SB, Fritton SP. 2012. Alterations in the osteocyte lacunar-canalicular microenvironment due to estrogen deficiency. *Bone* **51**:488–497 DOI 10.1016/j.bone.2012.05.014.

Sharma D, Larriera AI, Palacio-Mancheno PE, Gatti V, Fritton JC, Bromage TG, Cardoso L, Doty SB, Fritton SP. 2018. The effects of estrogen deficiency on cortical bone microporosity and mineralization. *Bone* **110**:1–10 DOI 10.1016/j.bone.2018.01.019.

Shipov A, Zaslansky P, Riesemeier H, Segev G, Atkins A, Shahar R. 2013. Unre-modeled endochondral bone is a major architectural component of the cortical bone of the rat (Rattus norvegicus). *Journal of Structural Biology* **183**:132–140 DOI 10.1016/j.jsb.2013.04.010.

Stern AR, Yao X, Wang Y, Berhe A, Dallas M, Johnson ML, Yao W, Kimmel DB, Lane NE. 2018. Effect of osteoporosis treatment agents on the cortical bone osteocyte microenvironment in adult estrogen-deficient, osteopenic rats. *Bone Reports* **8**:115–124 DOI 10.1016/j.bonr.2018.02.005.

Tomkinson A, Reeve J, Shaw RW, Noble BS. 1997. The death of osteocytes via apoptosis accompanies estrogen withdrawal in human bone. *Journal of Clinical Endocrinology & Metabolism* **82**:3128–3135.

Tommasini SM, Trinward A, Acerbo AS, De Carlo F, Miller LM, Judex S. 2012. Changes in intracortical microporosities induced by pharmaceutical treatment of osteoporosis as detected by high resolution micro-CT. *Bone* **50**:596–604 DOI 10.1016/j.bone.2011.12.012.

Vashishth D, Verborgt O, Divine G, Schaffler MB, Fyhrie DP. 2000. Decline in osteocyte lacunar density in human cortical bone is associated with accumulation of microcracks with age. *Bone* **26**:375–380 DOI 10.1016/S8756-3282(00)00236-2.

Wells G, Tugwell P, Shea B, Guyatt G, Peterson J, Zytaruk N, Robinson V, Henry D, O'Connell D, Cranney A, Grp OM, Grp ORA. 2002. Meta-analysis of the efficacy of hormone replacement therapy in treating and preventing osteoporosis in postmenopausal women. *Endocrine Reviews* **23**:529–539 DOI 10.1210/er.2001-5002.

Zarrinkalam MR, Mulaibrahimovic A, Atkins GJ, Moore RJ. 2012. Changes in osteocyte density correspond with changes in osteoblast and osteoclast activity in an osteoporotic sheep model. *Osteoporosis International* **23**:1329–1336 DOI 10.1007/s00198-011-1672-4.